Catalysis Today xxx (2016) xxx–xxx

Contents lists available at ScienceDirect

Catalysis Today

journal homepage: www.elsevier.com/locate/cattod

Nanostructured CeO_2 as catalysts for different AOPs based in the application of ozone and simulated solar radiation

E. Mena, A. Rey*, E.M. Rodríguez, F.J. Beltrán

Departamento de Ingeniería Química y Química Física, Universidad de Extremadura, Av. Elvas s/n, 06006 Badajoz, Spain

ARTICLE INFO

Article history:
Received 29 January 2016
Received in revised form 5 April 2016
Accepted 11 April 2016
Available online xxx

Keywords:
Nanostructured CeO_2
DEET
Ozone
Solar light
Photocatalytic ozonation

ABSTRACT

Two CeO_2 catalysts with different morphology (nanocubes and nanorods) were synthetized by hydrothermal treatment, characterized by TEM, XRD, N_2 adsorption-desorption isotherms, XPS and DR-UV–vis spectroscopy and examined for different AOPs (photocatalytic oxidation, catalytic and photocatalytic ozonation) using simulated solar radiation ($\lambda > 300$ nm) or visible radiation ($\lambda > 390$ nm) from a Xe lamp, and DEET as target compound. Neither significant DEET removal nor mineralization was achieved by solar photocatalysis and the catalysts did not show an important beneficial effect during catalytic ozonation. The best results were obtained in photocatalytic ozonation process being nanorods more active under visible radiation according to its lower band gap energy whereas nanocubes presented the highest intrinsic photocatalytic activity under visible and solar radiation. Photocatalytic ozonation of DEET with CeO_2 catalysts proceeds through a complex reaction mechanism that involves at least ozone-direct reaction that triggers a radical chain mechanism, indirect ozone reactions, ozone photolytic and photocatalytic decomposition and hydrogen peroxide formation-decomposition.

1. Introduction

Water pollution due to specific organic contaminants (phenolic compounds, aromatic hydrocarbons, pesticides, pharmaceuticals, etc.) is a growing problem that requires the implementation of advanced technologies capable of removing not only the initial compounds but also their metabolites. Among the available technologies, advanced oxidation processes (AOPs) have demonstrated to efficiently remove a wide variety of organic pollutants due to the generation of oxidizing species, mainly hydroxyl radicals, which non-selectively attack the organic matter [1]. Photocatalytic treatments are promising alternatives due to the possibility of using natural solar light as a radiation source to minimize treatment costs. Besides, the combination of photocatalysis with ozone (photocatalytic ozonation) increases the generation of oxidizing species leading to higher degrees of mineralization than individual treatments of ozonation or photocatalysis [2–4].

For the photocatalytic processes, much of the research effort is focused on the development of photocatalysts capable of effectively absorbing visible light in order to increase the fraction of usable solar radiation compared to the commonly used TiO_2 [5,6]. In this sense, cerium oxide CeO_2 is a wide band-gap semiconducting material usually in the range of 2.9–3.2 eV which absorbs light in the near UV and slightly in the visible region depending on the morphology and particle size, being its properties as catalyst and catalytic support highly shape-size dependent [7–9]. In addition, CeO_2 possesses a sufficiently long lifetime of photo-generated electron-hole pairs to trigger photocatalytic reactions in liquid and gas phase [10]. Bare CeO_2 with different morphologies/properties (microspheres, nanospheres, nanosheets, etc.) has been used as photocatalyst in the degradation of organic pollutants in water, most of them belonging to the dyes family [11–15] or phenol and phenol derivatives [8,16]. These works pointed out that the morphology and crystal size of CeO_2 are highly important in the amount and nature of surface defects, oxygen vacancies, CeO_2-light interaction and, definitely, in the behavior of CeO_2 as photocatalyst.

On the other hand, CeO_2 has demonstrated to be catalytically active during ozonation of organic pollutants of different nature such as phenol [17], oxalic and oxamic acids [18] or bezafibrate [19]. Main reaction pathways proposed are related to the adsorption and subsequent decomposition of ozone into hydroxyl radicals, being the presence of Ce(III)/oxygen vacancies in the surface the main responsible species of the catalytic activity [17,18].

As far as we know, the combination of photocatalytic oxidation with ozone using CeO_2 as photocatalyst has not been previously reported but it is expected to take benefits of both processes (pho-

* Corresponding author.
E-mail address: anarey@unex.es (A. Rey).

http://dx.doi.org/10.1016/j.cattod.2016.04.034
0920-5861/

tocatalysis and catalytic ozonation) together with the synergism observed during photocatalytic ozonation treatment [2]. Therefore, the aim of this work focuses on the application of two nanostructured CeO_2 catalysts with different morphology (nanocubes and nanorods) in ozone and photocatalysis based AOPs (photocatalysis, catalytic and photocatalytic ozonation) using simulated solar radiation (300–800 nm) and visible radiation (390–800 nm) from a Xe lamp, and *N*,*N*-diethyl-*meta*-toluamide (DEET) as target compound. DEET is a common insect repellent found in different aquatic environments [20], that presents a low reactivity with ozone [21], facilitating the comparison between the different processes.

2. Experimental

2.1. Catalysts preparation

Two CeO_2 catalysts were synthetized by hydrothermal treatment according to a previous work [22]. Briefly, $Ce(NO_3)_3{\cdot}6H_2O$ was dissolved in 6 M NaOH solution and then transferred to a 125 mL autoclave (filled at 75%) and heated during 24 h at 100 °C for nanorods (NR) or 180 °C for nanocubes (NC). After the hydrothermal treatment, the autoclave was cooling down to room temperature and then, the precipitates were separated by centrifugation, washed sequentially with water and ethanol and dried at 100 °C overnight.

2.2. Characterization

CeO_2 catalysts were characterized by different techniques. X-ray diffraction (XRD) patterns were recorded using a powder Bruker D8 Advance XRD diffractometer with a Cu Kα radiation (λ = 0.1541 nm). The data were collected from 2θ = 20°–80° at a scan rate of 0.02 s^{-1}. A Tecnai G2 20 (FEI Company) transmission electron microscope at 200 kV was used to study the crystallinity and morphology of the samples. Textural properties were analyzed by nitrogen adsorption–desorption isotherms at −196 °C using an Autosorb-1 apparatus (Quantachrome). The samples were outgassed at 250 °C for 12 h under vacuum (<10^{-2} mbar). Surface characterization was performed by X-ray photoelectron spectroscopy. XPS spectra were obtained with a Kα Thermo Scientific apparatus with Al Kα (hν = 1486.68 eV) X-ray source using a voltage of 12 kV under vacuum (2×10^{-7} mbar). Binding energies were calibrated relative to the C1s peak at 284.6 eV and spectra deconvolution was accomplished using XPS-Peak 4.1 software. Diffuse reflectance UV–vis spectroscopy (DR-UV–vis) measurements were performed with an UV–vis-NIR Cary-5000 spectrophotometer (Varian-Agilent Technologies) equipped with an integrating sphere device. Band gap values of the samples were obtained using Tauc's equation, assuming an indirect band gap semiconductor behavior [23].

2.3. Catalytic activity measurements

Photocatalytic experiments were carried out in a solar simulator (Suntest CPS, Atlas) provided with a 1500 W Xe lamp operated at 550 W m^{-2}. In some cases light transmission was restricted to λ > 390 nm by means of a modified polyester cut-off filter (Edmund Optics) for visible experiments whereas a window glass filter was used for simulating the spectrum of solar radiation reaching the Earth's surface (λ > 300 nm). The spectral irradiance of Xe lamp using the window glass filter, and the transmittance of the polyester filter are represented in Fig. 1. The experiments were carried out in semi-batch mode (batch with respect to the liquid phase and continuous with respect to the gas phase) using a borosilicate glass-made round flask provided with gas inlet, gas outlet and a liquid sampling port. In a typical photocatalytic ozonation experiment,

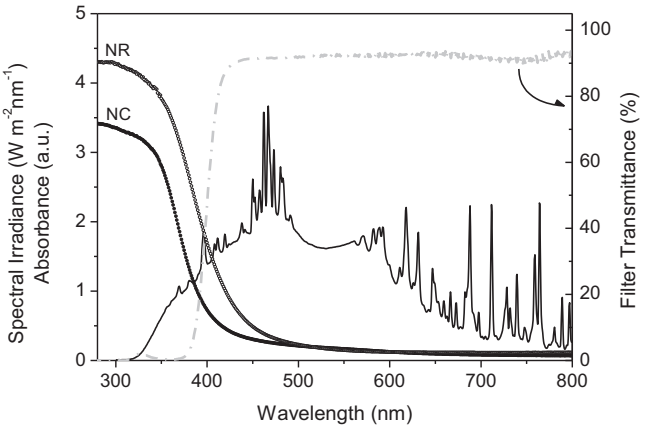

Fig. 1. UV–vis characteristics of the photocatalytic system applied (spectral irradiance of the Xe lamp in the solar simulator, transmittance of the UV filter and UV–vis absorbance of the CeO_2 catalysts).

the reactor was loaded with 500 mL of 5 mg L^{-1} of DEET aqueous solution (pH_0 = 6). The catalyst was then added (0.25 g L^{-1}) and the suspension was magnetically stirred in the dark for 30 min before switching on the lamp and feeding ozone to the reactor (15 L h^{-1} gas flow rate, 10 mg L^{-1} O_3, with an ozone generator (Labor-Ozonisator from Sander) fed with pure oxygen from a cylinder). The temperature in all the experiments was maintained at 35 °C. Besides photocatalytic ozonation ($CeO_2/O_3/h\nu$), blank experiments of photolysis (hν), single ozonation (O_3), photolytic ozonation ($O_3/h\nu$), adsorption (CeO_2), photocatalysis ($CeO_2/h\nu$) and catalytic ozonation (CeO_2/O_3) were carried out for comparative reasons. Most of the experiments were triplicated. Samples were withdrawn from the reactor at different interval times, filtered with 0.2 μm PTFE membranes and analyzed.

DEET concentration was analyzed by HPLC-DAD (Hitachi, Elite LaChrom) using a Phenomenex C-18 column (5 μm, 150 mm long, 3 mm diameter) and 0.6 mL min^{-1} of acetonitrile-acidified water (0.1% formic acid) as mobile phase (30–70 v/v, isocratic). Identification and quantification were carried out at 220 nm. Total organic carbon (TOC) was measured using a Shimadzu TOC-VSCH analyzer. Aqueous ozone was photometrically determined by the indigo method at 600 nm [24], in a UV–vis spectrophotometer Evolution 201 (Thermospectronic) and ozone in the gas phase was continuously monitored by an online analyzer (Anseros Ozomat GM-6000Pro). Hydrogen peroxide concentration was photometrically determined by the cobalt/bicarbonate method, at 260 nm using the same spectrophotometer [25]. Short-chain organic acids were analyzed by ion chromatography with chemical suppression (Metrohm 881Compact Pro) and a conductivity detector, using a MetroSep A sup 5 column (250 mm long, 4 mm diameter) at 45 °C and 0.7 mL min^{-1} of Na_2CO_3 from 0.6 to14.6 Mm in 50 min (10 min post-time for equilibration) as mobile phase.

3. Results and discussion

3.1. Photocatalysts characterization

The formation of nanostructured CeO_2 with NC or NR morphology was confirmed by TEM as can be observed in Fig. 2(A). From the NC images, also some rectangular prism particles have been detected (a minority in the images analyzed). The size of NC and NR, determined from several TEM representative images (not shown), is given in Table 1. A size distribution between 25 and 100 nm was obtained for NC whereas the NR presented a thickness of ~7.2 nm and lengths between 40 and 200 nm. NC and NR showed {100} and {110} + {100} exposed facets, respectively, which is in accordance

Please cite this article in press as: E. Mena, et al., Nanostructured CeO_2 as catalysts for different AOPs based in the application of ozone and simulated solar radiation, Catal. Today (2016), http://dx.doi.org/10.1016/j.cattod.2016.04.034

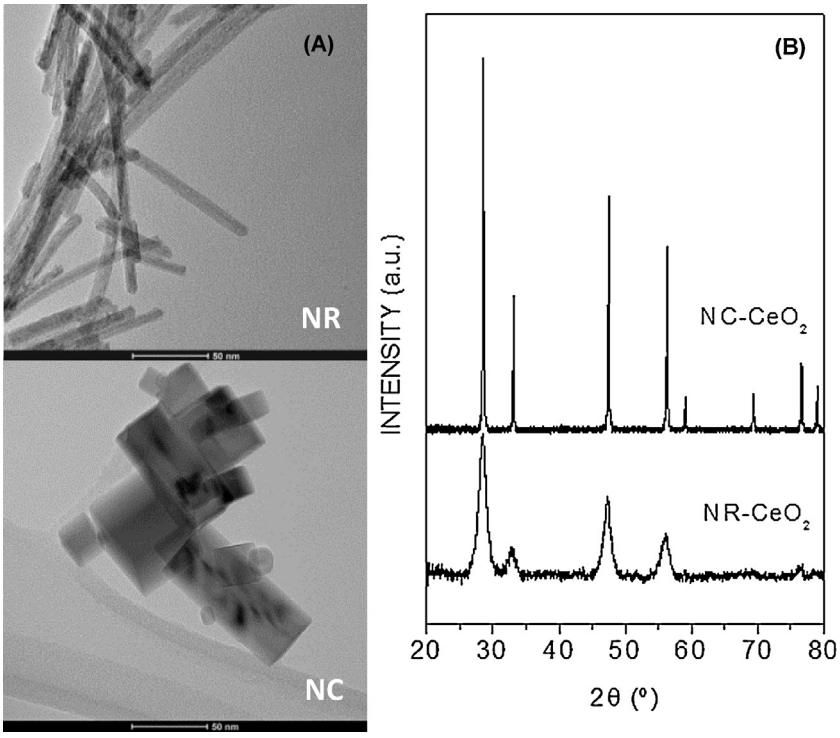

Fig. 2. Structural characterization of the CeO_2 nanostructured catalysts: (A) TEM images and (B) XRD patterns.

Table 1
Properties of the CeO_2 nanostructured catalysts.

Catalyst	Synthesis	[a]Size (nm)	Exposed facets	CeO_2 crystalline phase	S_{BET} ($m^2\ g^{-1}$)	V_p ($cm^3\ g^{-1}$)	[b]Ce(III) (%, at.)	[b]Ce(IV) (%, at.)	E_g (eV)
NC	Hydrothermal NaOH 6 M 180 °C, 24 h	25–100	{100}	Cubic	14	0.185	12.6	87.4	3.32
NR	Hydrothermal NaOH 6 M 100 °C, 24 h	(7.2 ± 1.1) x (40–200)	{110} + {100}	Cubic	109	0.522	23.6	76.4	3.07

[a] Size of the main dimensions by TEM analyses.
[b] Calculated from Ce 3d XPS deconvolution.

with previous reports [22]. On the other hand, XRD patterns shown in Fig. 2(B) confirmed the formation of pure CeO_2 cubic phase (fluorite structure, JCPDS 34-0394) in both NC and NR samples [22].

The porosity of the catalysts was evaluated by means of N_2 adsorption-desorption isotherms. BET surface area and total pore volumes are summarized in Table 1. Previous reports have shown that these materials are free of a developed pore structure except general random stacking of nanoparticles [22,26]. Due to its morphology and lower crystal size, NR presented higher S_{BET} and pore volume values than NC. With these characteristics, it is reasonable to assume that the powder dispersion of these materials (NR and NC) can be illuminated without internal shading from pores. Thus, the surface area exposed to light (S_{BET} in this case) should be taken into account since it can affect the photocatalytic behavior to some extent.

One of the main characteristics of CeO_2 catalysts is their oxygen and electron mobility due to the presence of surface defects, reduced states of Ce(III) or oxygen vacancies in the CeO_2 structure. High-resolution XPS spectra corresponding to Ce 3d spectral region of NC and NR samples have been plotted in Fig. 3. From this figure, a slight shift of Ce 3d peaks to lower binding energies in NR with respect to NC sample is noticed. This has been attributed to an increase of the electron density around Ce nucleus, suggesting the existence of more Ce(III) ions on the surface of NR sample [26]. In addition, this has been confirmed by the higher intensity of the peaks corresponding to Ce(III) species (v_0, v', u_0, u') in NR catalyst [18,26,27], leading to a higher percentage of surface Ce(III) in NR compared to NC sample (see Table 1).

Finally, optical properties of the catalysts have been studied by DR-UV–vis spectroscopy. Fig. 1 shows the absorbance UV–vis spectra of NC and NR where a noticeable shift to higher wavelength absorption for NR sample is observed, which suggests this catalyst can use a higher fraction of visible radiation to trigger photocatalytic reactions. The optical energy band gap values (E_g) calculated assuming indirect band gap behavior for both catalysts are also summarized in Table 1. A value of 3.32 eV was obtained for NC, somewhat higher to that reported for bulk CeO_2 (around 3.19 eV) due to smaller particle sizes [28]. On the contrary, a noticeable lower E_g value was calculated for NR indicating a clearly shift to higher absorption wavelengths as deduced from Fig. 1. This effect may be attributed to the lattice defects and oxygen vacancies present in the ceria NR [28], in agreement with the results obtained by XPS analyses.

3.2. Catalytic activity

The activity of the CeO_2 catalysts was evaluated in DEET degradation through AOPs of photocatalytic oxidation, catalytic ozonation and photocatalytic ozonation in aqueous solution using visible and simulated solar radiation in photocatalytic systems. The

Please cite this article in press as: E. Mena, et al., Nanostructured CeO_2 as catalysts for different AOPs based in the application of ozone and simulated solar radiation, Catal. Today (2016), http://dx.doi.org/10.1016/j.cattod.2016.04.034

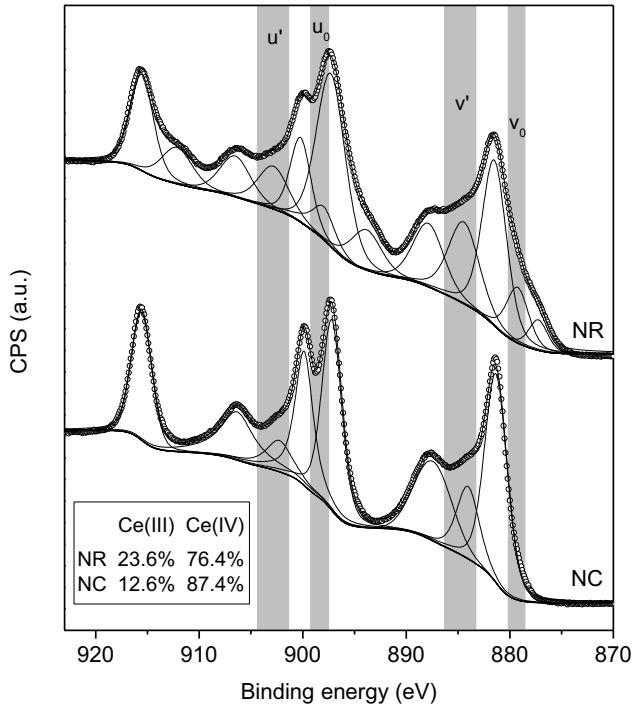

Fig. 3. High-resolution XPS spectra and deconvolution of the Ce 3d spectral region of the CeO_2 nanostructured catalysts.

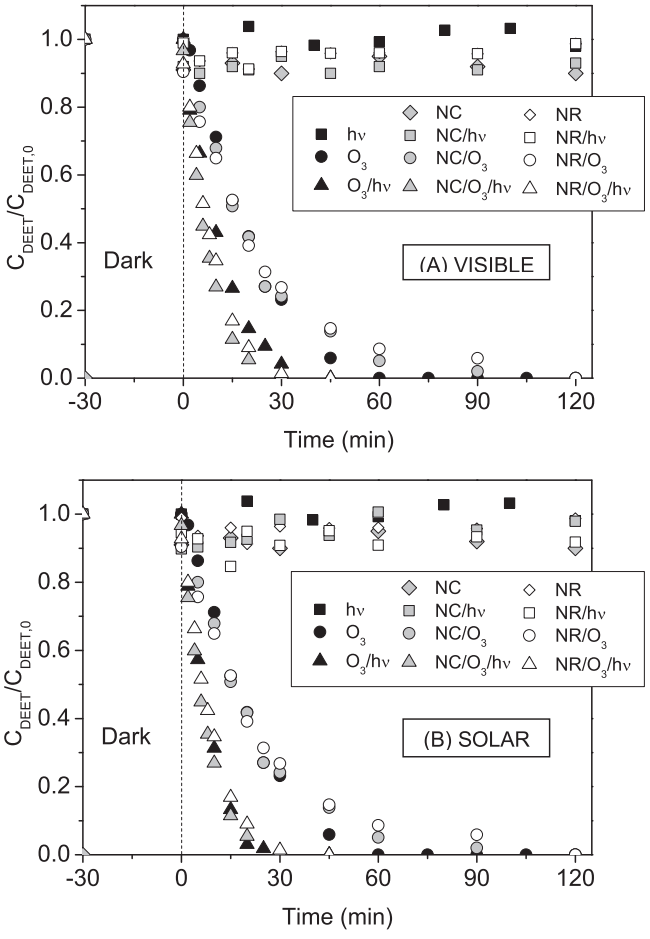

Fig. 4. Evolution of normalized DEET concentration during different treatments applied under visible (A) and solar (B) simulated radiation (maximum standard deviation of the normalized DEET concentrations in 3 repeated runs 0.03, not shown).

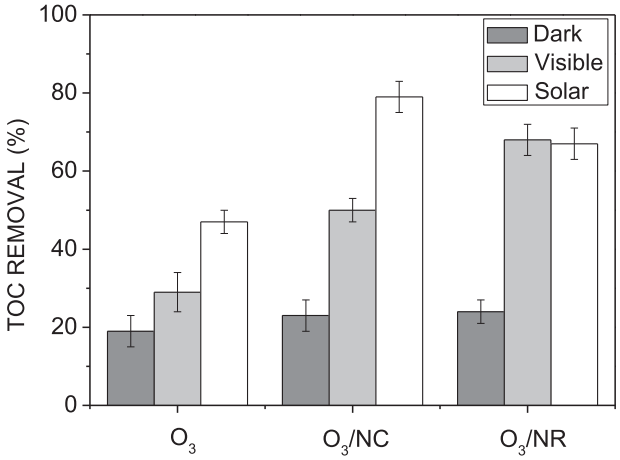

Fig. 5. TOC removal with the CeO_2 catalysts and O_3 processes.

results obtained for DEET degradation are shown in Fig. 4. Some blank experiments are also included for comparative purposes. As reported in a previous work, at the conditions applied no DEET degradation by direct photolysis was observed [29]. The adsorption capacity of both catalysts was also negligible being DEET removal lower than 10%. In addition, in spite of the optical properties of the catalysts, no significant DEET removal was achieved by photocatalysis regardless of the radiation used (visible or solar). These results differ from those previously reported using different CeO_2 catalysts, although in those cases photosensitizing dyes were used as target compounds [11–15]. On the other hand, the highest DEET degradation rate was obtained for ozone-based systems. Thus, single ozonation led to a complete removal of DEET in less than 60 min. A similar DEET evolution was observed during catalytic ozonation with respect to ozonation regardless of the catalyst used. This points out that these materials do not show any beneficial effect on DEET removal when combined with ozone in the dark, at the conditions used in this work.

However, the impact of the radiation (visible and solar) on the efficacy of ozone-based processes was significant and, in general, higher degradation rates were observed when solar light was used (Fig. 4(B)). In this sense, DEET was completely removed after 45 and 30 min when ozone was combined with visible and solar radiation, respectively, being these periods clearly lower than that required by single ozonation (60 min). It has been previously demonstrated that ozone can undergo direct photolysis under solar radiation promoting the formation of some reactive oxygen species capable of oxidizing the organic matter in aqueous solution [30,31]. Nevertheless, the interaction between visible radiation and ozone is unclear and will be investigated in future works. Finally, according to Fig. 4(A), the addition of NC and NR catalysts to the ozone + radiation system had almost no effect on DEET degradation rate. Only a slight beneficial effect was observed when visible light was used, regardless of the type of catalyst.

Main differences between ozone-based treatments were observed in terms of DEET mineralization (i.e. transformation into CO_2, H_2O and inorganic compounds). Fig. 5 shows the percentage of mineralization during ozone-based treatments at 120 min reaction time. As observed, ozone alone gave rise to only a 19% mineralization due to the formation of intermediate compounds refractory to ozone direct reaction (oxalic, formic and acetic acids were detected in the reaction medium) [32]. The presence of CeO_2 catalysts slightly increased (by 5%) the final mineralization, which could be attributable to a positive effect of cerium oxide on the elimination of some intermediate compounds formed during DEET ozonation. The combination of ozone and radiation gave rise to 29%

Please cite this article in press as: E. Mena, et al., Nanostructured CeO_2 as catalysts for different AOPs based in the application of ozone and simulated solar radiation, Catal. Today (2016), http://dx.doi.org/10.1016/j.cattod.2016.04.034

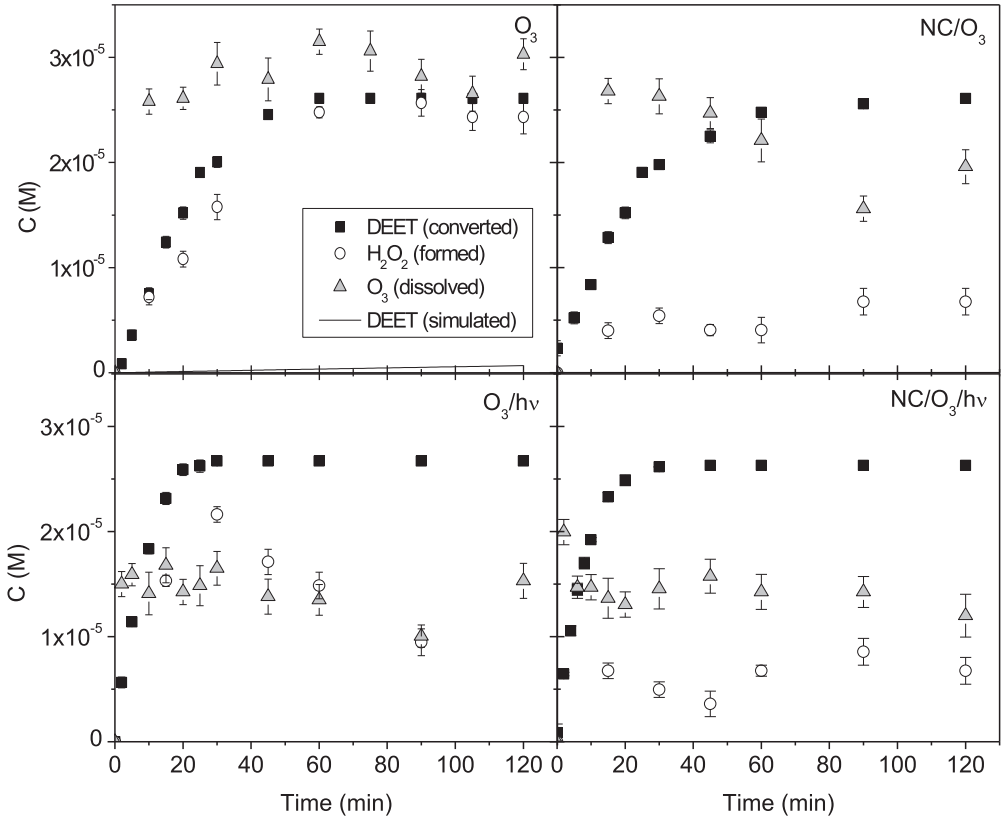

Fig. 6. Evolution of DEET converted, H_2O_2 formed and O_3 dissolved during the O_3 treatments applied using CeO_2-NC catalyst and simulated solar light.

Table 2
Pseudo-first order apparent rate constant for TOC elimination during photocatalytic ozonation runs.

Catalyst	Radiation	$k_{TOC} \times 10^3$ (min^{-1})	$k_{TOC}/S_{BET} \times 10^4$ ($min^{-1}\ m^{-2}\ g$)	R^2
NC	Visible	7.2	5.1	0.98
	Solar	11.8	8.4	0.96
NR	Visible	11.2	1.1	0.95
	Solar	11.5	1.1	0.94

and 47% of TOC removal under visible and solar light, respectively. Therefore, compared to visible the effect of the entire solar spectrum (including wavelengths between 300 and 390 nm) is much higher. However, the best results were obtained when photocatalytic ozonation was applied, being NR the most active under visible radiation (68% TOC removal), likely due to its lower band gap energy as a consequence of higher Ce(III) surface ratio, whereas NC presented the highest photocatalytic activity under solar radiation (80% TOC removal). This is in agreement with the highest energy of {100} facets (thermodynamically more unstable) predominant in NC with respect to NR, allowing higher photocatalytic activity for this material due to once excited, the photoinduced holes exhibit superior oxidizing ability, according to previously reported results [26].

These results have also been confirmed by calculating the pseudo-first order apparent rate constant of TOC removal, k_{TOC}, during photocatalytic ozonation treatment, according to Eq. (1):

$$-\frac{dTOC}{dt} = k_{TOC}TOC \quad (1)$$

where TOC is expressed in mg L^{-1}, t in min and k_{TOC} in min^{-1}. Results are summarized in Table 2 together with the correlation coefficient. Taking into account the different irradiated surface area of the two catalysts (see Table 1), normalized to S_{BET} apparent rate constants (k_{TOC}/S_{BET}, $min^{-1}\ m^{-2}\ g$) have been calculated. The values obtained (Table 2) confirm the highest photocatalytic activity of ceria NC. It is also noticeable that solar UV radiation did not improve the mineralization rate when NR is used probably due to an increase of the recombination rate in the semiconductor.

3.3. Considerations on the reaction mechanism of DEET photocatalytic ozonation with CeO_2 catalysts and solar radiation

According to the above results, photocatalytic ozonation of DEET using the CeO_2 catalysts studied here, may proceed through a complex mechanism with the expected participation of ozone (direct reaction), and/or HO• radicals formed from ozone decomposition (indirect reactions). Ozone can decompose into HO• by several pathways: (1) in the dark, (2) by interaction with light, (3) by interaction with the catalyst, and (4) by interaction with both light and the catalyst. To discuss the possible contributions of each pathway Fig. 6 shows the evolution of DEET eliminated, dissolved ozone and hydrogen peroxide formed during ozone-based treatments using NC CeO_2 and simulated solar radiation.

Regarding to ozone-direct reactions, a low reactivity of DEET towards ozone has been previously reported ($k_{O3\text{-}DEET} = 0.123\ M^{-1}\ s^{-1}$ [21]). Taking into account this value, at the conditions used in this work, the reaction between ozone and DEET progress into the slow kinetic regime [32,33], being DEET degradation rate by direct ozone reaction given by Eq. (2):

$$-\left(\frac{dC_{DEET}}{dt}\right) = k_{O3-DEET}C_{DEET}C_{O3} \quad (2)$$

where C_{DEET} is DEET molar concentration and C_{O3} is dissolved ozone molar concentration. The expected evolution of DEET eliminated during ozonation in the dark considering only its reaction with ozone is shown in Fig. 6. As it is observed, the experimental conver-

sion rate was much higher than that predicted by Eq. (2), indicating that species different than O_3 are the main responsible for the degradation of the target compound. However, it is important to notice that $k_{O3\text{-}DEET}$ value was reported at 20 °C whereas the temperature during the experiments reaches 35 °C. Also, due to the low value of $k_{O3\text{-}DEET}$ some uncertainty on its determination should not be disregarded.

During all ozone-based treatment initial pH evolved from 6 to 4.5-4. At these pH values, at the beginning of the experiment, some ozone decomposition can be promoted by hydroxide anion although it likely becomes negligible when pH decreases [32]. Therefore, during DEET degradation by single ozonation in the dark it can be hypothesized that direct interaction between DEET-O_3 acts as a trigger of a chain mechanism that leads to the formation of ozonide and/or HO• radicals, as has been previously reported for different organic compounds [33]. The key role of HO• during DEET single ozonation has been previously reported [34].

The evolution of dissolved O_3, also depicted in Fig. 6, shows a higher accumulation during ozonation compared to treatments where catalyst and/or radiation were also present. This is indicative of the decomposition of ozone over the catalyst surface (although almost inefficient in the dark) and/or through its photolysis. According to literature [30,35], both mechanisms could promote the formation of hydroxyl radicals, thus increasing the mineralization rate of DEET.

In addition, it is well known that hydrogen peroxide is commonly formed through direct ozone and hydroxyl radical reactions. Accordingly, H_2O_2 was detected during DEET ozonation. As observed in Fig. 6, during single ozonation, about the same concentration of H_2O_2 is formed respect to DEET depleted. When light and/or NC catalyst were also present, the ratio between H_2O_2 in solution and DEET eliminated was much lower, and more markedly in the presence of NC thus indicating the decomposition of H_2O_2 is accelerated by CeO_2 catalyst surface. It is important to notice that H_2O_2 decomposition seems to be inefficient towards DEET degradation and mineralization according to the evolution of DEET and TOC during catalytic ozonation (dark). However, the role of H_2O_2 as electron acceptor during solar light photocatalytic ozonation using CeO_2 cannot be disregarded [35]. The role of hydrogen peroxide as electron acceptor as well as the contribution of the different reaction pathways to DEET degradation and mineralization by photocatalytic ozonation using solar light and CeO_2 NC as catalyst will be the subject of future work.

4. Conclusions

Nanostructured CeO_2 catalysts with different morphology (nanorods and nanocubes) were active in photocatalytic ozonation treatment of DEET under visible and simulated solar radiation. CeO_2 with nanorod-like structure presented higher irradiated surface area due to its morphology and also higher amount of surface defects and oxygen vacancies, leading to smaller band gap energy, and thus being apparently more active than CeO_2 nanocubes under visible light radiation. However, the presence of the exposed facets {100} in CeO_2 nanocubes provokes an increased intrinsic photocatalytic activity in this material with respect to nanorods under both visible and solar radiation. Photocatalytic ozonation of DEET with CeO_2 catalysts proceeds through a complex reaction mechanism that involves at least an ozone-direct reaction that triggers a radical chain mechanism, indirect ozone reactions, ozone photolytic and photocatalytic decomposition and hydrogen peroxide formation-decomposition. The importance of the different processes and the effect of visible radiation will be the subject of a future work.

Acknowledgements

Authors thank the Spanish MINECO/European Feder Funds (CTQ2012-35789-C02-01) and Junta de Extremadura (Ayuda Exp. GR15-033) for economic support. E. Mena thanks the Consejería de Empleo, Empresa e Innovación (Junta de Extremadura) and European Social Fund for her FPI grant (Ref. PD12059).

References

[1] M.A. Oturan, J.J. Aaron, Crit. Rev. Environ. Sci. Technol. 44 (2014) 2577–2641.
[2] T.E. Agustina, H.M. Ang, V.K. Vareek, J. Photochem. Photobiol. C Photochem. Rev. 6 (2005) 264–273.
[3] M. Mehrjouei, S. Müller, D. Möller, Chem. Eng. J. 263 (2015) 209–219.
[4] J. Xiao, Y. Xie, H. Cao, Chemosphere 121 (2015) 1–17.
[5] S. Malato, P. Fernández-Ibáñez, M.I. Maldonado, J. Blanco, W. Gernjak, Catal. Today 147 (2009) 1–59.
[6] S.Y. Dong, J.L. Feng, M.H. Fan, Y.Q. Pi, L.M. Hu, X. Han, M.L. Liu, J.Y. Sun, J.H. Sun, RSC Adv. 5 (2015) 14610–14630.
[7] W. Huang, Y. Gao, Catal. Sci. Technol. 4 (2014) 3772–3784.
[8] M. Aslam, M.T. Qamar, M. Tahir-Soomro, I.M.I. Ismail, N. Salah, T. Almeelbi, M.A. Gondal, A. Hameed, Appl. Catal. B Environ. 180 (2016) 391–402.
[9] X. Huang, M.J. Beck, Chem. Mater. 27 (2015) 5840–5844.
[10] M.D. Hernández-Alonso, A.B. Hungría, A. Martínez-Arias, M. Fernández-García, J.M. Coronado, J.C. Conesa, J. Soria, Appl. Catal. B Environ. 50 (2004) 167–175.
[11] W. Deng, D. Chenn, L. Chenn, Ceram. Int. 41 (2015) 11570–11575.
[12] S.K. Muduli, S. Wang, S. Chen, C. Fan-Ng, C.H.A. Huan, T.C. Sum, H.S. Soo, Beilstein J. Nanotechnol. 5 (2014) 517–523.
[13] Y. Yu, Y. Zhu, M. Meng, Dalton Trans. 42 (2013) 12087–12092.
[14] T. Feng, X. Wang, G. Feng, Mater. Lett. 100 (2013) 36–39.
[15] A.B. Sifontes, M. Rosales, F.J. Méndez, O. Oviedo, T. Zoltan, J. Nanomater. (2013) 1–9 (Article ID265797).
[16] C. Karunakaran, R. Dhanalakshmi, Sol. Energy Mater. Sol. Cells 92 (2008) 1315–1321.
[17] M.F.P. da Silva, L.S. Soeira, K.R.P. Daghastanli, T.S. Martins, I.M. Cuccovia, R.S. Freire, P.C. Isolani, J. Therm. Anal. Calorim. 102 (2010) 907–913.
[18] P.C.C. Faria, J.J.M. Orfao, M.F.R. Pereira, Catal. Commun. 9 (2008) 2121–2126.
[19] A.G. Gonçalves, J.J. Orfao, M.F.R. Pereira, Environ. Technol. 36 (2015) 776–785.
[20] W.A. Adams, C.A. Impellitteri, J. Photochem. Photobiol. A Chem. 202 (2009) 28–32.
[21] F.J. Benítez, J.L. Acero, J.F. García-Reyes, F.J. Real, G. Roldán, E. Rodríguez, A. Molina-Díaz, Ind. Eng. Chem. Res. 52 (2013) 17064–17073.
[22] H.X. Mai, L.D. Sun, Y.W. Zhang, R. Si, W. Feng, H.P. Zhang, H.C. Liu, C.H. Yan, J. Phys. Chem. B 109 (2005) 24380–24385.
[23] J. Tauc, Mater. Res. Bull. 5 (1970) 721–729.
[24] H. Bader, J. Hoigné, Water Res. 15 (1981) 449–456.
[25] W. Masschelein, M. Denis, R. Ledent, Water Sewage Works (August) (1977) 69–72.
[26] D. Jiang, W. Wang, L. Zhang, Y. Zheng, Z. Wang, ACS Catal. 5 (2015) 4851–4858.
[27] M.J. Muñoz-Batista, M.N. Gómez-Cerezo, A. Kubacka, D. Tudela, M. Fernández-García, ACS Catal. 4 (2014) 63–72.
[28] J. Zdravkovic, B. Simovic, A. Golubovic, D. Poleti, I. Veljkovic, M. Scepanovic, G. Brankovic, Ceram. Int. 141 (2015) 1970–1979.
[29] E. Mena, A. Rey, S. Contreras, F.J. Beltrán, Catal. Today 252 (2015) 100–106.
[30] L. Sánchez, X. Domènech, J. Casado, J. Peral, Chemosphere 50 (2003) 1085–1093.
[31] D.H. Quiñones, A. Rey, P.M. Álvarez, F.J. Beltrán, P.K. Plucinski, Appl. Catal. B Environ. 144 (2014) 96–106.
[32] F.J. Beltran, Ozone Reaction Kinetics for Water and Wastewater Systems, CRC Press, Boca Raton, Florida (USA), 2004.
[33] A. Rey, E. Mena, A.M. Chávez, F.J. Beltrán, F. Medina, Chem. Eng. Sci. 126 (2015) 80–90.
[34] J.L. Acero, F.J. Benítez, F.J. Real, E. Rodríguez, Water Air Soil Pollut. 226 (2015) 139-1–139-14.
[35] E. Mena, A. Rey, B. Acedo, F.J. Beltrán, S. Malato, Chem. Eng. J. 204–206 (2011) 131–140.

Please cite this article in press as: E. Mena, et al., Nanostructured CeO_2 as catalysts for different AOPs based in the application of ozone and simulated solar radiation, Catal. Today (2016), http://dx.doi.org/10.1016/j.cattod.2016.04.034